

Available online at [www.sciencedirect.com](http://www.sciencedirect.com)

Chinese Journal of Aeronautics 21(2008) 313–319

**Chinese  
Journal of  
Aeronautics**[www.elsevier.com/locate/cja](http://www.elsevier.com/locate/cja)

# Low-velocity Impact Damage Analysis of Composite Laminates Using Self-adapting Delamination Element Method

**Wang Lipeng, Yan Ying\*, Wu Dafang, Wu Hao***School of Aeronautic Science and Engineering, Beijing University of Aeronautics and Astronautics, Beijing 100083, China*

Received 21 August 2007; accepted 25 January 2008

## Abstract

On the basis of a 2D 4-node Mindlin shell element method, a novel self-adapting delamination finite element method is presented, which is developed to model the delamination damage of composite laminates. In the method, the sublaminates elements are generated automatically when the delamination damage occurs or extends. Thus, the complex process and state of delamination damage can be simulated practically with high efficiency for both analysis and modeling. Based on the self-adapting delamination method, linear dynamic finite element damage analysis is performed to simulate the low-velocity impact damage process of three types of mixed woven composite laminates. Taking the frictional force among sublamination during delaminating and the transverse normal stress into account, the analytical results are consistent with those of the experimental data.

**Keywords:** self-adapting delamination element method; low-velocity impact; delamination; composite laminate

## 1 Introduction

Poor transverse property is one of the serious disadvantages of the composite laminates. As a result, invisible inner damages occur easily inside the laminate, especially the delamination damage that reduces the residual mechanical properties remarkably. At present, mainly two kinds of methods are used to model the delamination damage of composite laminates in finite element analysis (FEA) method. One is the stiffness degradation method<sup>[1–4]</sup>, in which the material properties in the delaminated region are being reduced to model the influence of delamination. This method is mostly used in 3D FEA model. The other one is the 2D multi-element model<sup>[5–9]</sup>, in which the multi-layer 2D elements are used to model the delamination damage, and penalty function or spring element is used to avoid unrea-

sonable separation or penetration of the two layers of delamination. Although the second method is logical, it is inconvenient for modeling because it needs to estimate the area that has a high possibility of delamination to set multi-layer elements there, and it is inefficient in calculation because of the huge degree of freedom (DOF).

In this article, a self-adapting delamination element method based on the 2D 4-node Mindlin shell element is presented to model the generation and expansion of a composite laminate's delamination damage by generating sublaminates element automatically. A dynamic FEA program is developed to analyze the delamination damage process of mixed woven composites under low-velocity impact.

## 2 Finite Element Method

### 2.1 Self-adapting delamination element method

In the general self-adapting element method,

\*Corresponding author. Tel.: +86-10-82315947.

E-mail address: [yingyan@buaa.edu.cn](mailto:yingyan@buaa.edu.cn)

Foundation item: National Natural Science Foundation of China (50073002)

the density of elements can be increased automatically; thus, the modeling effort can be reduced and the discretization can be controlled automatically. Consequently, the efficiency of analysis, including the modeling, and precision of calculations can be increased. Based on the same conception, a novel self-adapting delamination element method is presented in this article, so that the complex delamination damage process and state of delamination can be simulated practically with high efficiency.

In the 2D shell FEA model, every node has five degrees of freedom (DOFs), including  $u$ ,  $v$ ,  $w$ ,  $\theta_x$ , and  $\theta_y$ . Among them,  $u$  and  $v$  are the in-plane DOF, whereas  $w$ ,  $\theta_x$ , and  $\theta_y$  are the transverse DOF. Fig.1 shows one of the transverse sections of a laminate along its thickness, and the laminate is modeled by shell FEA model along its middle plane. Elem 3 is a normal 2D quadrilateral element without delamination and nodes  $B$  and  $C$  are two of its four nodes.

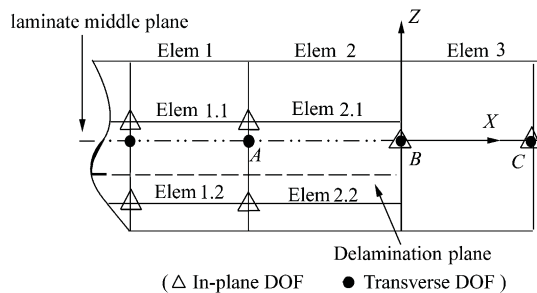


Fig.1 DOF in the self-adapting delamination element.

When the delamination occurs in Elem 1 and Elem 2, the laminate is divided into two parts; also, the two elements will be divided into four subelements including Elem 1.1, Elem 1.2, Elem 2.1, and Elem 2.2. Each of those four subelements can be treated as a separated shell element in the following analysis. Accordingly, the element before delaminating is called mother element. During damaging under the low-velocity impact, there is no separation and penetration between the two layers of delamination; therefore, the upper and lower parts have the same flexibility and angle of rotation having the same transverse DOF. However, because of the sliding along the delamination plane, the two parts have different in-plane DOF. Therefore, when de-

lamination occurs, transverse DOF of node  $A$  remains unchanged, but its in-plane DOF increases to two sets,  $u_1$ ,  $v_1$  and  $u_2$ ,  $v_2$ , which represent the in-plane DOF of upper and lower parts, respectively. When calculating the stiffness matrix of the upper subelements, such as Elem 1.1 or Elem 2.1, five degrees of freedom,  $u_1$ ,  $v_1$ ,  $w$ ,  $\theta_x$ , and  $\theta_y$  of node  $A$  will be used. Another set of DOF,  $u_2$ ,  $v_2$ ,  $w$ ,  $\theta_x$ , and  $\theta_y$  will be used when calculating the stiffness matrix of the lower subelements, such as Elem 1.2 or Elem 2.2. Consequently, when there are  $n$  delamination planes near a node, the node will have  $n+1$  sets of in-plane DOF and one set of transverse DOF; thus, the node will have  $2n+5$  DOF totally. Because the number of subelements and DOF can be changed automatically during analysis, the FEA method has the ability of self-adapting, and that is why it is named as self-adapting delamination element. The FEA model used in this method is shown in Fig.2, where the broken lines denote the delamination planes and the heavy black lines denote the shell elements before delaminating or sublaminates elements after delaminating. It is obvious that the complex delamination process and state can be modeled exactly by the self-adapting delamination element method.

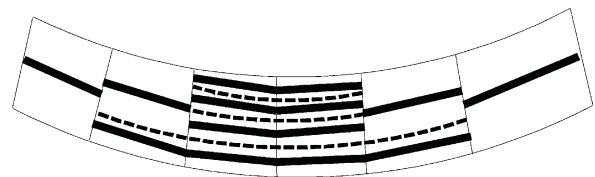


Fig.2 Schematic self-adapting delamination element model.

In this method, the delaminating process is treated as two steps, delamination of element and delamination of node. Whether the delamination of element occurs is judged by the delamination criterion of the laminate based on its stress state. The delamination of node happens only when all the elements that are sharing the node has been delaminated at the same interface. In Fig.1, it can be deduced that, delamination of node does not happen in node  $B$ . Therefore, node  $B$  has only five DOF,  $u$ ,  $v$ ,

$w$ ,  $\theta_x$ , and  $\theta_y$ , the same as node  $C$ . The DOFs used to calculate the stiffness matrices of subelement Elem 2.1 and Elem 2.2 are  $u + h_1\theta_x$ ,  $v + h_1\theta_y$ ,  $w$ ,  $\theta_x$ ,  $\theta_y$ , and  $u + h_2\theta_x$ ,  $v + h_2\theta_y$ ,  $w$ ,  $\theta_x$ ,  $\theta_y$ , respectively; among them  $h_1$  and  $h_2$  are used to satisfy the condition of displacement compatibility near the delamination crack tip. They stand for the distances between the middle planes of Elem 2.1 and Elem 2.2 to the middle plane of their mother elements, Elem 2. For complex delamination cases, the displacement fields of the subelements near the crack tip and the velocity and acceleration fields associated with the dynamic analysis can all be determined in the same way by the condition of displacement compatibility. The total DOF number changes after the delamination of the node, therefore, the stiffness matrix, the mass matrix and displacement, and velocity and acceleration vectors in dynamic analysis must be rebuilt based on the new DOF number.

Essentially, the self-adapting delamination element method models the delamination damage by multi-layer elements. However, only one layer of the element is needed at the beginning of the analysis because multi-layer elements can be generated automatically. Therefore, the method is convenient for modeling. Additionally, it does not need to estimate the delamination area before setting multi-layer elements as required for the 2D multi-element model<sup>[5-9]</sup>. Moreover, the multi-layer subelements generated from the same mother element use the same set of transverse DOF, thus avoiding unreasonable separation and penetration between the subelements and reducing the number of total DOF. Therefore, the present self-adapting delamination element method is highly efficient for both modeling and calculation.

## 2.2 Dynamic FEA method

On the basis of the Hamilton theory, the dynamic differential equation of composite laminates using FEA method is

$$M\ddot{U} + C\dot{U} + KU = F \quad (1)$$

where  $M$ ,  $C$ , and  $K$  are the mass, damping, and stiffness matrices, respectively;  $U$ ,  $\dot{U}$ , and  $\ddot{U}$  are

the displacement, velocity, and acceleration vectors, and  $F$  is the applied load vector.

The density and stiffness of the impactor are much higher than those of the laminates and its deformation is very small during impacting, therefore, it can be treated as a mass point. The contact force is defined by the modified Hertzian contact law<sup>[4,10-12]</sup>. The damping matrix is defined by the Rayleigh damping model.

The FEA model adopted in this study, which is built with the commercial FEA software, MSC. Patran, has a length of 150 mm and width of 100 mm and is divided into 432 four-node shell elements. According to the experiment state<sup>[13-14]</sup>, the model is simply supported by the DOF of  $z$  direction of all nodes on the edges of a rectangle of 127.2 mm  $\times$  76.2 mm. All the analysis process and graphical post-processing are performed by a self-developed program.

## 3 Damage Analyses

There is no damage in the model laminates before being impacted and during impacting. The Hashin criterion is used for the analysis to judge the appearance and expansion of the damage of fiber and matrix. The modified stiffness reducing method presented in Ref.[4] is used to analyze the influence of fiber and matrix damage.

### 3.1 Delamination damage criteria

Because bidirectional woven plies in the mixed woven composite laminates are being studied here, for the woven ply,  $\sigma_{23}$  and  $\sigma_{33}$  that induce the matrix crack damage must be ignored, and  $\sigma_{23}/\sigma_{33}$  is considered as having the same effect as  $\sigma_{11}/\sigma_{13}$ . Based on these considerations the author presented the delamination damage criterion for mixed woven composites in Ref.[12]. However, using 3D FEA method in that study for the transverse stress component of the laminate was not accurate, because the continuous stress condition could not be satisfied<sup>[13]</sup>. As a result, the inhibition effect of transverse compressive stress on the delamination was exaggerated. In the present study, the criterion is modified as fol-

lows: the inhibition effect of the transverse compressive stress on the delamination is ignored when  $-Z_C \leq \sigma_{33}^n < 0$ . The modified delamination damage criteria are:

(1) When both the upper and lower plies are unidirectional plies, if  $\sigma_{33}^n < -Z_C$  or  $\sigma_{33}^n \geq 0$ , then

$$e_d^2 = D_a \left[ \left( \frac{\sigma_{23}^n}{S_i^n} \right)^2 + \left( \frac{\sigma_{13}^{n+1}}{S_i^{n+1}} \right)^2 + \left( \frac{\sigma_{22}^{n+1}}{Y_i^{n+1}} \right)^2 + \left( \frac{\sigma_{33}^n}{Z^n} \right)^2 \right] \quad (2)$$

In Eq.(2), when  $\sigma_{33}^n \geq 0$ ,  $Z^n = Z_T^n$ ; otherwise,  $Z^n = Z_C^n$ .

If  $-Z_C \leq \sigma_{33}^n < 0$ , then

$$e_d^2 = D_a \left[ \left( \frac{\sigma_{23}^n}{S_i^n} \right)^2 + \left( \frac{\sigma_{13}^{n+1}}{S_{i13}^{n+1}} \right)^2 + \left( \frac{\sigma_{22}^{n+1}}{Y_i^{n+1}} \right)^2 \right] \quad (3)$$

In these two equations, the stresses are along the main direction of every ply; the superscript  $n$  and  $n+1$  denote the lower and upper plies near interface plane; the subscript  $i$  denotes the situ strength; and  $D_a$  is an empirical material parameter presented by Chang<sup>[1]</sup> and  $D_a = 2.5$  in this study.

(2) When the upper is woven ply and lower is unidirectional ply, if  $\sigma_{33}^n < -Z_C$  or  $\sigma_{33}^n \geq 0$ , then

$$e_d^2 = D_a \left[ \left( \frac{\sigma_{13}^{n+1}}{S_{i13}^{n+1}} \right)^2 + \left( \frac{\sigma_{22}^{n+1}}{Y_i^{n+1}} \right)^2 + \left( \frac{\sigma_{33}^n}{Z^n} \right)^2 \right] \quad (4)$$

If  $-Z_C \leq \sigma_{33}^n < 0$ , then

$$e_d^2 = D_a \left[ \left( \frac{\sigma_{13}^{n+1}}{S_{i13}^{n+1}} \right)^2 + \left( \frac{\sigma_{22}^{n+1}}{Y_i^{n+1}} \right)^2 \right] \quad (5)$$

(3) When the upper is a unidirectional ply and lower is woven ply, if  $\sigma_{33}^n < -Z_C$  or  $\sigma_{33}^n \geq 0$ , then

$$e_d^2 = D_a \left[ \left( \frac{\sigma_{23}^n}{S_{i23}^n} \right)^2 + \left( \frac{\sigma_{13}^{n+1}}{S_{i13}^{n+1}} \right)^2 + \left( \frac{\sigma_{22}^{n+1}}{S_{i23}^{n+1}} \right)^2 + \left( \frac{\sigma_{33}^n}{Z^n} \right)^2 \right] \quad (6)$$

If  $-Z_C \leq \sigma_{33}^n < 0$ , then

$$e_d^2 = D_a \left[ \left( \frac{\sigma_{23}^n}{S_{i23}^n} \right)^2 + \left( \frac{\sigma_{13}^{n+1}}{S_{i13}^{n+1}} \right)^2 + \left( \frac{\sigma_{22}^{n+1}}{S_{i23}^{n+1}} \right)^2 \right] \quad (7)$$

(4) When both the upper and lower plies are woven plies, if  $\sigma_{33}^n < -Z_C$  or  $\sigma_{33}^n \geq 0$ , then

$$e_d^2 = D_a \left[ \left( \frac{\bar{\sigma}_{13}}{S_{i13}^{n+1}} \right)^2 + \left( \frac{\bar{\sigma}_{23}}{S_{i23}^{n+1}} \right)^2 + \frac{\sigma_{33}^n{}^2}{Z^n} \right] \quad (8)$$

If  $-Z_C \leq \sigma_{33}^n < 0$ , then

$$e_d^2 = D_a \left[ \left( \frac{\bar{\sigma}_{13}}{S_{i13}^{n+1}} \right)^2 + \left( \frac{\bar{\sigma}_{23}}{S_{i23}^{n+1}} \right)^2 \right] \quad (9)$$

The stress components of the last two equations are average values. Delamination damage will occur when  $e_d \geq 1$ .

### 3.2 Transverse normal stress analysis

The transverse normal stress needs to be considered in the delamination criteria, but it cannot be obtained directly in 2D shell FEA method. In this study, the transverse normal stress is calculated on the basis of the stress equilibrium condition near the impact point. It is assumed that only the four elements near impact point are influenced by the transverse normal stress.

The cylinder shown in Fig.3 is a small part of the laminate near impact point. Its height is the thickness of the laminate, its radius  $r = a/\sqrt{2}$ , is the distance from impact point to the central points of the surrounding four elements, and  $a$  is the length of side of these four elements. When the inertial force is ignored, a static stress equilibrium equation can be defined as

$$\pi r^2 \sigma_{33} = \int_0^z 2\pi r \tau_{rz} dz \quad (10)$$

The transverse shear stress  $\tau_{rz}$  is calculated by the method presented in Ref.[15].

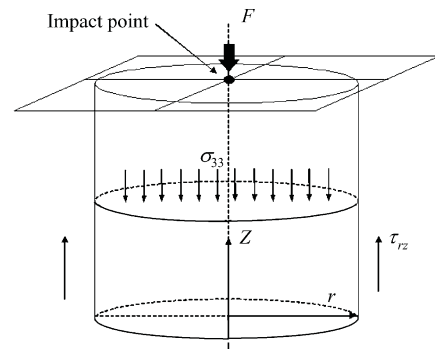


Fig.3 Transverse normal stress near the impact point.

## 4 Examples

Three typical mixed woven composite laminates studied in experiments in Refs.[13-14] are analyzed using the self-adapting delamination ele-

ment method in this study. The constructions of these laminates are shown in Table 1. The impacting process and damage area of every laminate under the impact energy of 2.23 J/mm, 4.45 J/mm, and 6.67 J/mm are analyzed.

**Table 1 Ply stacking sequence of mixed woven composites**

| Laminate | Ply stacking sequence*  | Ply number | Thickness/mm | Proportion of 0° unidirectional tape/% |
|----------|---|------------|--------------|--|
| P-3      | $[(\pm 45)_2/0/(\pm 45)_2/0/(\pm 45)/0/(\pm 45)/90]_s$                        | 20         | 4.52         | 21.24                                  |
| P-4      | $[(\pm 45)/0/(\pm 45)/0_2/(\pm 45)/0_2/(\pm 45)/90/\bar{0}]_s$                | 21         | 4.24         | 41.51                                  |
| P-8      | $[(\pm 45)/0_2/(\pm 45)/0_2/(\pm 45)/0_2/(\pm 45)/0_2/(\pm 45)/90/\bar{0}]_s$ | 29         | 5.74         | 47.40                                  |

\* $(\pm 45)$  shows as a woven fabric ply which is laid at a 45° angle relative to the main direction; 0 or 90 shows as a tape ply which is laid along or perpendicular to the main direction.

### 4.1 Interface friction

Frictional force certainly exists between the rough interfaces of sublaminations after delaminating. The impact force obtained from analysis will be markedly lower than that obtained from experiment if the frictional force is being ignored, as shown in Fig.4.

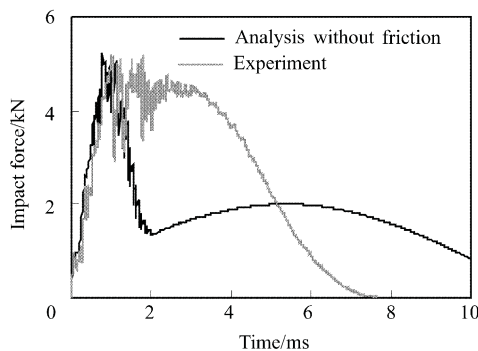


Fig.4 Impact force without considering the interface friction (P-4, 4.45 J/mm).

In the low-velocity impact problem of laminates, the relative slide of the sublaminates is so small that the friction can be treated as static friction. As it is difficult to get the accurate friction coefficient, a simple spring element is used to model the frictional force.

In this study, the stiffness of the spring element is thought to be directly proportional to the area controlled by the spring element and the impact force that is corresponding to the interface pressure. So:

$$k = \alpha \cdot A \cdot F_I \quad (11)$$

where  $k$  is the stiffness of the spring element,  $A$  the area controlled by the spring element,  $F_I$  the impact force, and  $\alpha$  an undetermined empirical coefficient and  $\alpha = 5.5 \times 10^7 \text{ m}^2/\text{s}$  in this study.

### 4.2 Results of analysis

Using dynamic FEA method based on the self-adapting delamination element method, the typical impact force-time response curves are obtained and compared with the experimental results as shown in Figs.5-7. The impact force curves can be obviously

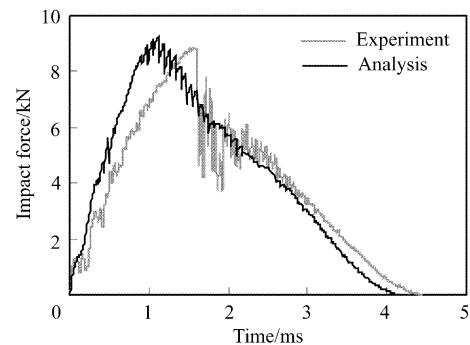


Fig.5 Impact force-time response curve (P-8, 2.23 J/mm).

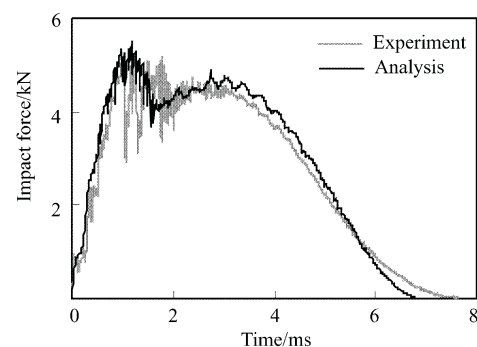


Fig.6 Impact force-time response curve (P-4, 4.45 J/mm).

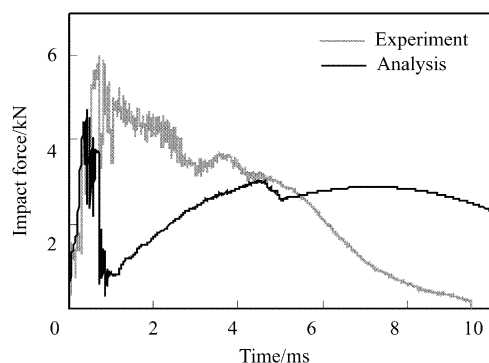


Fig.7 Impact force-time response curve (P-3, 6.67 J/mm).

divided into three phases. They are contact phase, damage phase, and rebound phase. Because of the happening and expanding of the damage during the damage phase, the impact force curve fluctuates within a certain range, whereas, this situation did not happen during the other phases.

It shows that the results of analysis are consistent with those of experiments for different laminates under the impact energies of 2.23 J/mm and 4.45 J/mm. When the impact energy is much higher, such as 6.67 J/mm, significant error occurs. The reasons are many-sided. One of the most important reasons is that the damage becomes more serious around the impact point resulting in higher flexibility of the laminate, therefore, it becomes a geometrical nonlinear problem and the bending stiffness is reduced in the present linear dynamic analysis, which induces significant error finally.

The damage areas in Table 2 show that when the impact energy is not higher than 4.45 J/mm, the analytical results are very well consistent with the

**Table 2 Resultant damage area of analysis and experiment**

| Laminate | Impact energy/(J·mm <sup>-1</sup> ) | Delamination area/mm <sup>2</sup> |          | Error/% |
|----------|-------------------------------------|-----------------------------------|----------|---------|
|          |                                     | Experiment                        | Analysis |         |
| P-3      | 2.23                                | 467±56                            | 485.9    | 4.0     |
|          | 4.45                                | 635±57                            | 549.9    | -13.4   |
|          | 6.67                                | 1 189±88                          | 850.6    | -28.5   |
| P-4      | 2.23                                | 462±56                            | 452.4    | -2.1    |
|          | 4.45                                | 683±115                           | 710.4    | 4.0     |
|          | 6.67                                | 1 162±339                         | 943.6    | -18.8   |
| P-8      | 2.23                                | 630±71                            | 598.9    | -4.9    |
|          | 4.45                                | 1 132±158                         | 938.4    | -17.1   |

experimental results and the errors are within the range of the dispersion of the experimental data. It is shown in Fig.8 that the damage shape of the analytical result is elliptical, which agrees well with the experimental result.

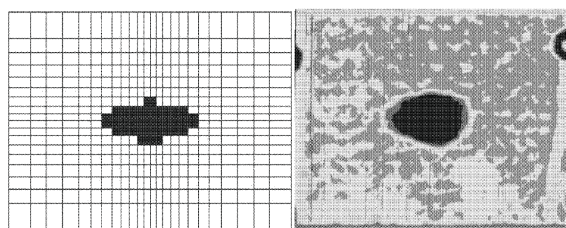


Fig.8 Resultant damage shape of analysis and experiment (P-4, 4.45).

## 5 Conclusions

(1) A novel self-adapting delamination element method that has been developed to model the delamination damage of composite laminates is presented in this article. In this method, the sublaminates elements are generated automatically when the delamination damage occurs or extends. Thus, the complex process and state of delamination damage can be simulated practically with high efficiency for both analysis and modeling efforts.

(2) In the self-adapting delamination element method, the sublaminates from one mother element have the same transverse DOF but different in-plane DOFs to avoid the unreasonable separation and penetration between the upper and lower sublaminates, and also to improve the calculating efficiency.

(3) The modified delamination criteria for mixed woven composite are presented in this article.

(4) The interface friction influences the impact damaging process remarkably. Spring element is used to model the friction and the analytical results agreed with the experimental results very well. However, it is necessary to do more theoretical work on this issue.

(5) On the basis of the FEA method presented in this article, the dynamic FEA is performed for different laminates under different impact energy levels. Accurate impact force-time curves, damage areas, and damage shapes are obtained.

(6) Mainly because of the serious bending caused by the serious damage near the impact point under higher impact energy, there will be large errors in linear analysis in which the geometrical nonlinear feature is ignored.

## References

- [1] Choi H Y, Chang F K. A model for prediction damage in graphite/epoxy laminated composites resulting from low-velocity point impact. *Journal of Composite Materials* 1992; 26(14): 2134-2169.
- [2] Guan Z D. Low-velocity impact and damage process of composite laminates. *Journal of Composite Materials* 2002; 36(7): 851-871.
- [3] Cheng G, Li Z N, Kou C H. Finite element analysis of low-velocity impact damage of stitched laminates. *Journal of Reinforced Plastics and Composites* 2004; 23(9): 987-995.
- [4] Zeng D. Study on low velocity impact properties of stitched composites and aircraft structure flutter model design. Beijing: Beijing University of Aeronautics and Astronautics, 2006. [in Chinese]
- [5] Reedy E D, Mello F J, Guess T R. Modeling the initiation and growth of delaminations in composite structures. *Journal of Composite Materials* 1997; 31(8): 812-831.
- [6] Johnson A F, Pickett A K. Impact and crash modeling of composite structures. *European Conference Computational Mechanics (ECCM'99)*. 1999.
- [7] Johnson A F, Pickett A K, Rozycki P. Computational methods for predicting impact damage in composite structures. *Composites Science and Technology* 2001; 61(15): 2183-2192.
- [8] Tay T E, Tan V B C, Deng M. Element-failure concepts for dynamic fracture and delamination in low-velocity impact of composites. *International Journal of Solids and Structures* 2003; 40(3): 555-571.
- [9] Greve L, Pickett A K. Delamination testing and modeling for composite crash simulation. *Composites Science and Technology* 2006; 66(6): 816-826.
- [10] Sun C T. Dynamic response of anisotropic laminated plates under initial stress to impact of a mass. *Journal of Applied Mechanics* 1975; 693-698.
- [11] Yang S H, Sun C T. Indentation law for composite law for composite laminates. *Composite Materials: Testing and Design, ASTM STP 787*. 1982: 425-449.
- [12] Wang L P, Yan Y, Zeng D. Finite element analysis on low-velocity impact damage of mixed woven composites. *Acta Aeronautica et Astronautica Sinica* 2007; 28(S): S121-S124. [in Chinese]
- [13] Wang L P, Yan Y. Experimental study of stiffness, strength and low-speed impact performance on mixed woven composites. *Acta Aeronautica et Astronautica Sinica* 2006; 27(5): 851-855. [in Chinese]
- [14] Wang L P, Yan Y, Zeng D, et al. Influence of thickness to low-speed impact and static transverse compress performance of mixed woven composites. *Acta Aeronautica et Astronautica Sinica* 2007; 28(1): 213-216. [in Chinese]
- [15] Rolfes R, Rohwer K. Improved transverse shear stresses in composite finite elements based on first order shear deformation theory. *International Journal for Numerical Methods in Engineering* 1997; 40(1): 51-60.

## Biographies:

**Wang Lipeng** Born in 1979, he is a Ph.D. candidate. His research interests are finite element modeling and impact properties of composite structures.  
E-mail: hbwlp@ase.buaa.edu.cn

**Yan Ying** Born in 1963, she is a professor. Her research interests include aircraft structural design, damage/fracture mechanics of composite materials, failure modeling, textile structure composites, damage detection, environmental effects on the behavior of composites, impact and postimpact compression, repair of composite laminates and structures.

**Wu Dafang** Born in 1950, he is a professor. His research interest includes experimental mechanics.

**Wu Hao** Born in 1981, he is a Ph.D. candidate. His research interest is structure optimization.